IN-SILICO CHARACTERIZATION AND DESIGN OF NANOPORE-BASED DNA SEMICONDUCTOR SEQUENCING DEVICES

California Institute of Technology

Andres Jaramillo-Botero, Qi An, and William A. Goddard

Midterm report, FY2

THE SAIT DESIGN

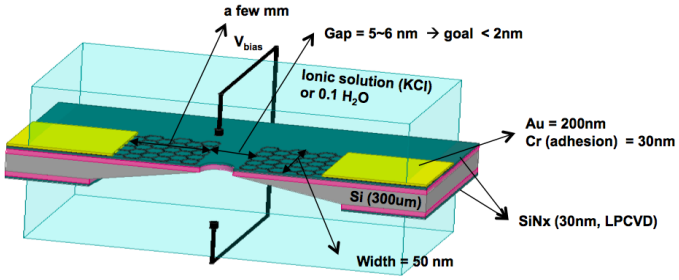

FIGURE 1 SAMSUNG SAIT NANOSEQUENCING DEVICE DESIGN

The device models explore the idea of measuring the electron tunneling current across ssDNA nucleobases as they translocate in solution through a solid-state nanopore configured as shown in Figure 1 (Samsung SAIT design). The experimental device analyzed here contains a set of graphene nanoribbons (GNR) as electrodes, separated by a gap of 5nm, and sitting on top of a silicon-nitride substrate.

Here, we report on the electronic transport properties of the nucleobases, from a first-principles based analysis using Quantum Mechanics (QM) Density Functional Theory (DFT) and the Non-Equilibrium Green's Function (NEGF) method, and on the translocation control of ssDNA across the pore using Molecular Dynamics simulations. We have also begun analyzing a similar configuration but with Cr electrodes, considering the difficulties in experimentally fixing the graphene nanoribbons on top of SiNx substrate. Partial results on their transport properties are described within.

ELECTRONIC TRANSPORT ACROSS NUCLEOBASES

We focused on confirming that: (1) there is a sufficient difference in the transmission/conductance spectra G(V) of individual nucleobases to allow them to be distinguished from one another, (2) that the measured conductance for a single nucleobase is independent of its orientation as it passes through the pore, and 3) on analyzing the transmission eigenstates at the transmission spectra peaks.

Electronic structure calculations using DFT LDA-PZ with a double-zeta-polarized basis set were used to determine the transverse electrical current for the different model systems with optimized geometry; starting with ideal hydrogen-capped zigzag GNR electrodes. The following configurations were tested:

1. Electrode tips are sharp and all nucleobases placed at 1.7 Angstroms from the two electrodes, with absorption atoms in each base chosen according to their natural hydrogen bonding states in DNA (see Figure 2). With this configuration we studied the effect of repulsive interactions on the system's geometry, in particular on the nucleobase orientation with respect to the electrodes. Sharp-edged GNRs have been demonstrated experimentally by [1]
2. Electrode tips are flat and 2nm apart (as expected from the SAIT design). The nucleobase's geometric center was chosen to be at the inter-electrode geometric center and their alignment, again, according to their natural hydrogen bonding states in DNA (see YY).
3. Electrode tips are flat and placed 1nm apart to improve signal to noise ratio. The nucleobase's geometric center is placed at the center of the center distance between electrodes. Planar and perpendicular orientations were tested.
4. Functionalized zigzag graphene electrode tips using a hydrogen-bond grabber was tested on one base.

An additional configuration, replacing the zigzag GNR electrodes by armchair GNR electrodes is being tested for different ribbon widths. Here we present the results for a single width. We believe that conductivity may be improved in the armchair-GNR metallic state, versus the zigzag, due to the ___. The electronic states of GNRs depend on the edge structures. Zigzag edges provide the edge-localized state with non-bonding molecular orbitals near the Fermi energy. Zigzag GNRs are always metallic while armchairs can be either metallic or semiconducting, depending on their width. Armchair nanoribbons are semiconducting with an energy gap scaling with the inverse of the GNR width and experimental results show that the energy gaps do increase with decreasing GNR width. Both results by tight-binding(TB) method [2-5] and first-principles calculations [6-9] [16–19] show that spectra of GNRs depend strongly on the shapes of their edges.

The different configurations allow us to study the molecule's transmission spectrum, and other electronic transport properties, at 0V bias and at finite biases as a function of inter-electrode distance. We expect a shift in magnitude, but not in overall transmission distribution, as a function of inter-electrode gap distance. Furthermore, we expect close-range repulsive interactions to affect the orientation of the nucleotide with respect to the electrodes at 0V bias. For the planar and perpendicular setups, we expect to reduce base geometry and orientation dependencies.

GNR MOLECULAR STRUCTURE MODELS

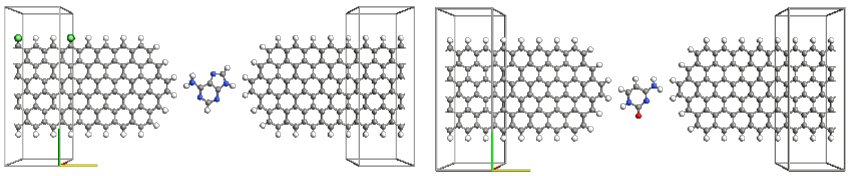

adenine cytosine

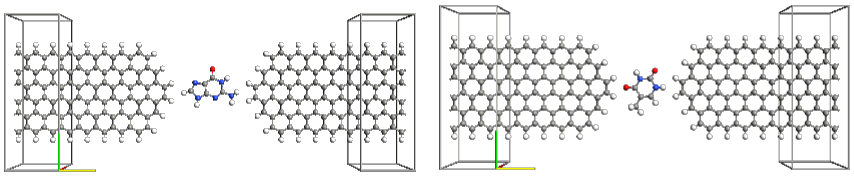

guanine thymine

FIGURE 2 NUCLEOBASE-GNR ELECTRODES SETUP 1.

Configurations from Figure 2 end up distorted after optimization, suggesting that narrow gaps (<1nm) without probe functionalization will not work appropriately.

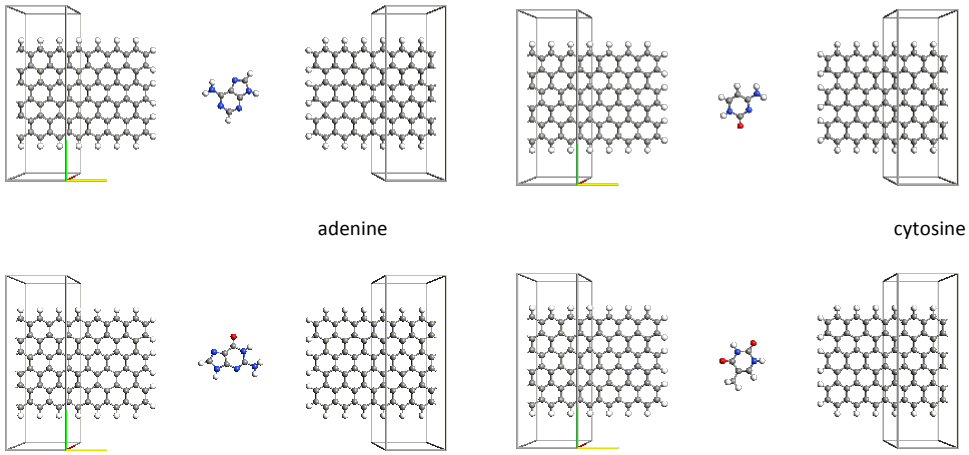

adenine cytosine

guanine thymine

FIGURE 3 NUCLEOBASE-GNR ELECTRODES SETUP 2.

Figure 3 devices have no transmission spectra at 0 bias for ssDNA, nor over a finite bias range of -3.6:3.6V (i.e. flat IV curve), due to the large 2nm gap separating the GNR electrodes (basis set dies off quickly after ~8 Angstroms and no ghost atoms were used in our calculations). High bias voltages may be used to provide a tunneling current signature, albeit it would be unrealistic to apply such high potentials on DNA.

Configurations from Figure 4 represent some of the workable designs (e.g. zigzag versus armchair electrodes and functionalized electrode tips for improved base conductivity) and alternate states (i.e. base orientation) for measuring transmission across the molecular base junction of a ssDNA. Results for transmission spectra and further electronic structure calculations on these are discussed below.

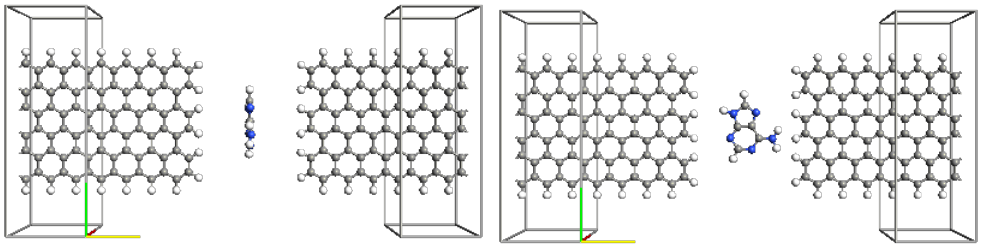

a) b)

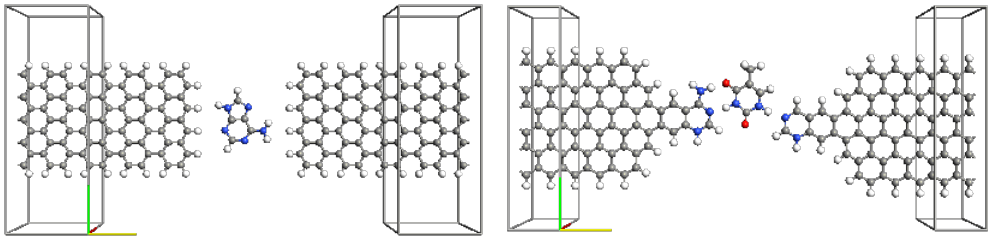

c) d)

FIGURE 4 ADDITIONAL CONFIGURATIONS TESTED (ONLY SHOWING NUCLEOBASE A), INCLUDE: (A) PERPENDICULAR BASE TRANSLOCATION ON A 1NM GAP, (B) PARALLEL BASE TRANSLOCATION ON 1NM GAP, AND (C) ARMCHAIR GNR ELECTRODES AT 1NM GAP, AND (D): NITROGEN-FUNCTIONALUZED TIPS WITH H-BOND GRABBERS.

ZERO-BIAS CALCULATIONS

TRANSMISSION SPECTRUM AND DEVICE DENSITY OF STATES

Calculations were performed using Density Functional Theory (DFT) with LDA exchange correlation and a PZ functional and a double zeta polarize LCAO basis set. Electron temperature was set to 300K. Geometries were optimized using a Quasi-Newton optimizer with convergence criteria set to a threshold force of 0.1eV/Angstroms and a maximum step size of 0.5 Angstroms. Transmission spectra were calculated self-consistently (required only for biased systems) over an energy range of -5:5 E/eV using a Monhorst Pack grid with 1x1x101 k-point sampling in x,y,z directions, respectively, were z is the transmission direction. All two-probe tunneling calculations were performed as described in our report for FY1.

Figure 3 devices have no transmission spectra at 0 bias, nor over a finite bias range of -3.6:3.6V (i.e. flat IV curve), due to the large 2nm gap separating the GNR electrodes (basis set dies off quickly after ~8 Angstroms). High bias voltages may be used to provide a tunneling current signature, albeit it would be unrealistic to apply such high potentials on DNA.

Figure 5 shows the transmission spectrum for each of the bases in the perpendicular arrangement with respect to the GNR electrode plane, according to a 0V bias and the setup depicted in Figure 2. For adenine, there are ~4 distinguishable narrow peaks, at around -5, -4.5, -3.5, and 2.1 eV. None rise above T(E)=1. Cytosine has narrow peaks at 2.2eV and -4.5eV, and a broad peak between -3 and 4eV. Guanine shows a single narrow peak at -3.9eV and Thymine two broad peaks between -3 and 5eV and a larger narrow peak at ~5eV. The magnitude of transmission is significantly lower, for the same GNR electrode gap distance, compared to the parallel arrangement results, shown in Figure 6. This is expected, since the probability of electron tunneling is proportional to distance and of course, electron orbital and density overlap. We also observe additional peaks in the spectra of Figure 6, which may indicated nucleobase orientation-dependence with respect to the GNR electrodes. Nevertheless, a perpendicular translocation of bases is expected to have reduced orientation dependencies, albeit it is less probable (from our MD translocation results, below) that this extreme will occur.

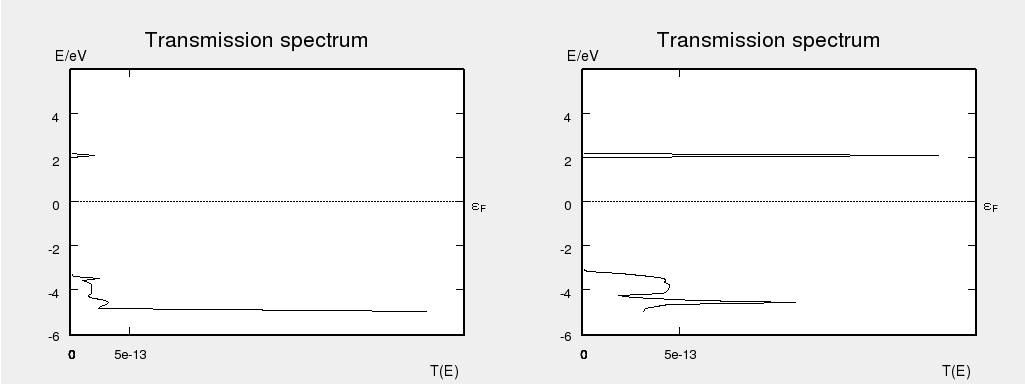

adenine cytosine

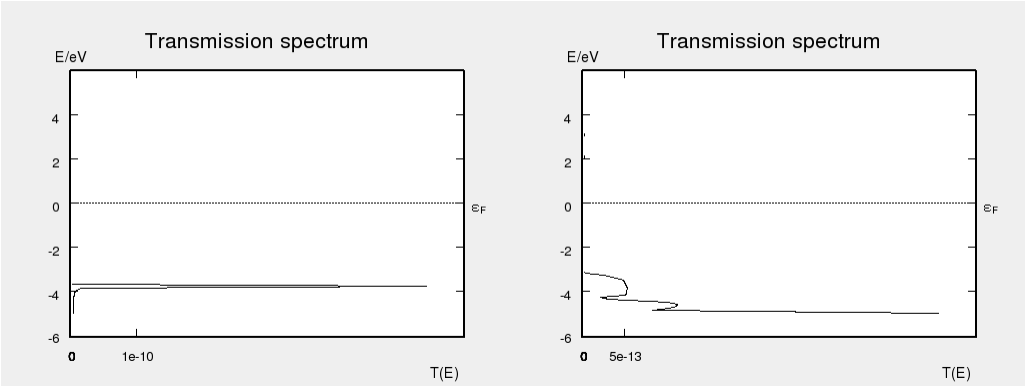

guanine thymine

FIGURE 5 0V BIAS TRANSMISSION SPECTRUM FOR THE CORRESPONDING CASES IN FIGURE 4A (I.E. 1NM GAP AND PERPENDICULAR BASE CONFIGURATION). TRANSMISSION SIGNATURES ARE DISTINCT, ALBEIT SMALL IN MAGNITUDE AT 0V BIAS (LARGEST TRANSMISSION IN GUANINE AT ~-4V).

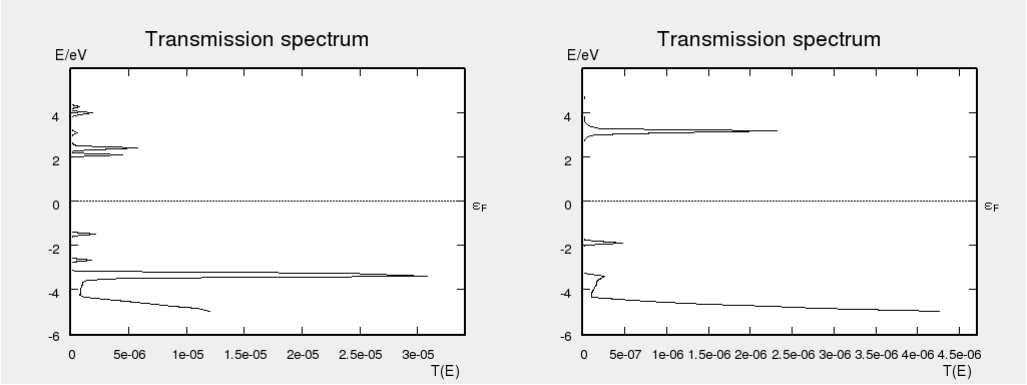

adenine cytosine

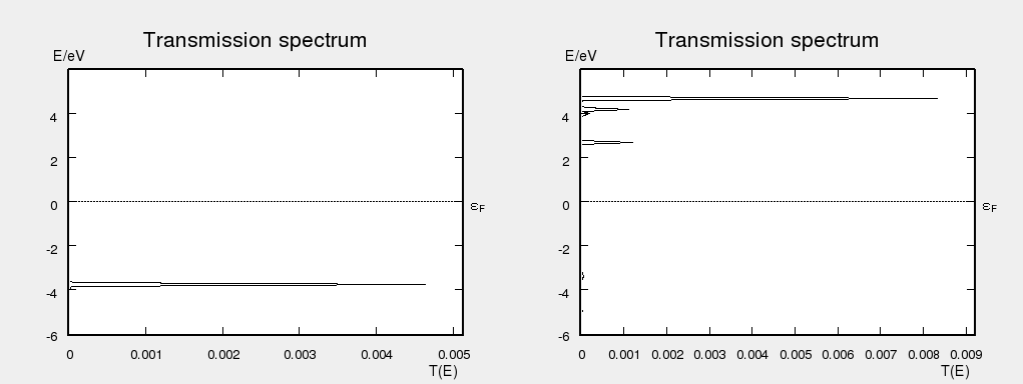

guanine thymine

FIGURE 6 0V BIAS TRANSMISSION SPECTRUM FOR THE CORRESPONDING CASES IN FIGURE 4B (I.E. 1NM GAP AND PARALLEL BASE CONFIGURATION).

From Figure 7 (armchair GNR electrodes), we note that the transmission peaks are mostly narrow banded for all nucleobases and appear to be at similar energy levels as those shown in Figure 6 (for zigzag GNR electrodes), except the former has improved transmission magnitudes. As mentioned, armchair GNRs may be semiconducting or metallic, depending on their width (chirality).

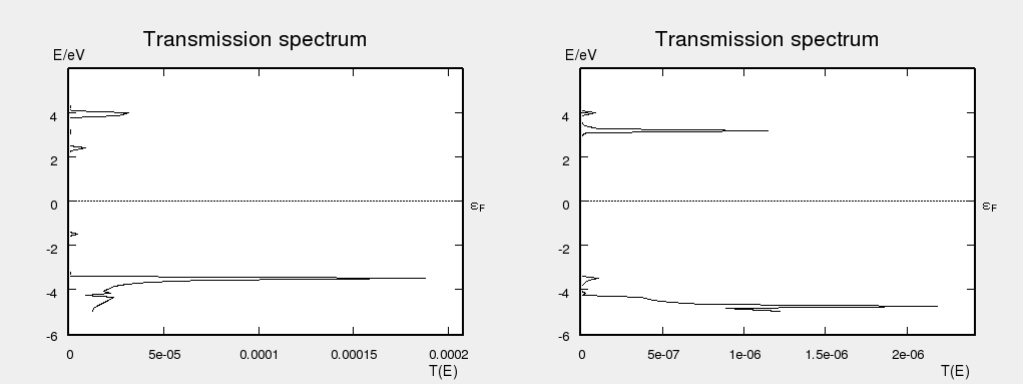

adenine cytosine

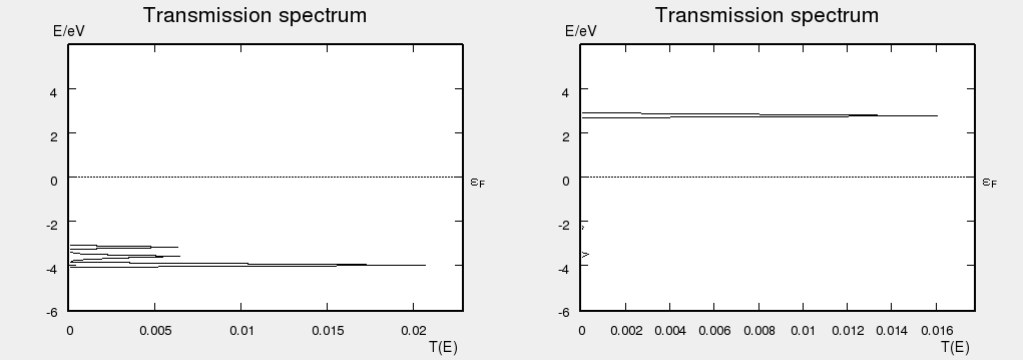

guanine thymine

FIGURE 7 0V BIAS TRANSMISSION SPECTRUM FOR THE CORRESPONDING CASES IN FIGURE 4C (I.E. 1NM GAP, PARALLEL NUCLEOBASES WITH ARMCHAIR GNR ELECTRODES).

Using these results, we are now calculating the projected Device Density of States (DDOS) for each configuration to determine the correspondence between the energy levels on the nucleobase and the

transmission spectrum, i.e. remove electrode transmission effect. To further understand the energy levels of the nucleobases in the presence of the surrounding electrodes, we are also calculating the diagonal component of the self-consistent Hamiltonian (i.e. the molecular projected self-consistent Hamiltonian (MPSH)). This involves projecting the individual nucleobase atoms (i.e. removing the electrode atoms) and mapping the resulting energy states to those in the range of correspondence with the transmission spectrum (TS). We then use the corresponding states to calculate each eigenstate, for each quantum number, found from the MPSH-TS correspondence. By visualizing the eigenstates together with the corresponding optimized geometry we will determine the HOMO and LUMO states for each nucleobase.

We will proceed to determine the transmission eigenvalues by diagonilizing the transmission matrix. The number of resulting eigenvalues will indicate the number of individual transmission channels through the molecule, and the eigenvalue the strength of each channel. We will focus on the largest eigenvalues per energy.

Finally, we will select the two highest transmission eigenstates per energy to determine the highest transmission probability across each GNR electrode configuration and compute the Local Device Density of States (LDDOS) averaged over the transmission plane of the molecule to determine the electronic density distribution.

We have also computed transmission probabilities for a N-functionalized zigzag GNR-based device, as shown in Figure 8. We confirmed geometry stability (i.e. optimization) of the hydrogen-bonded adenine on the H-bond grabber N-functionalized electrodes. H-bonds were ~1.97Angstroms.

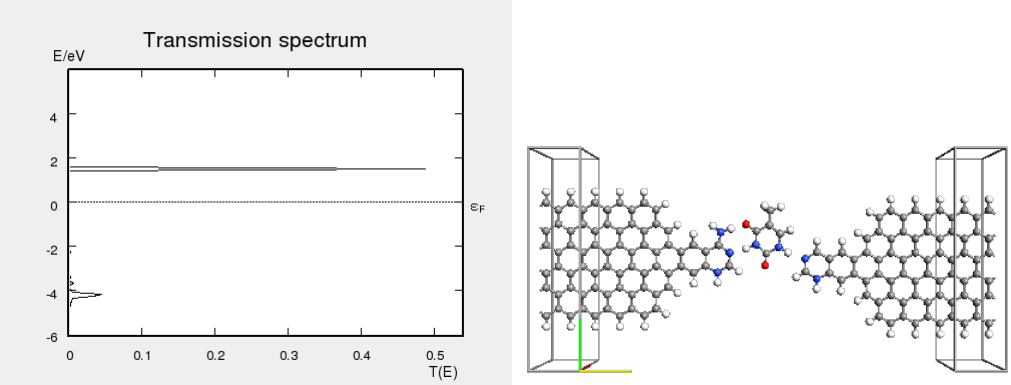

FIGURE 8 0V BIAS TRANSMISSION SPECTRUM FOR ADENINE USING FIGURE 4D CONFIGURATION (SHOWN TO THE RIGHT, I.E. N-FUNCTIONALIZED GNR ZIGZAG ELECTRODES) SHOW SIGNIFICANTLY ENHANCED TRANSMISSION PEAKS CENTERED AROUND 1.8EV (UP TO 50% TRANSMISSION PROBABILITY) AND -4EV ENERGIES.

IV CHARACTERISTICS

This section is currently being in progress, except for the 2nm gap systems, which resulted in no IV response within the bias voltage range used (-3.6 to 3.6V). Each system requires over 3 weeks of calculation over a bias voltage range of -3.6:3.6V on an 8-CPU core node. We are currently using the MIO DFTB parameter set for organic systems (H,C,N,O,S,P) to improve our throughput in electronic structure calculations. The target is to complete the electronic structure and MD translocation loop using MD trajectories, as proposed initially.

IV CURVES, LDDOS AND VOLTAGE DROP ACROSS MOLECULAR JUNCTION

This section is still work in progress.

CHROMIUM GAP DEVICES

We have started building the Cr based devices for characterization, according the SAIT's design.

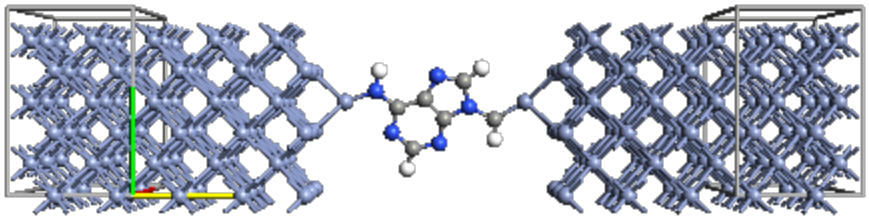

FIGURE 9 CHROMIUM-BASED ELECTRODES (ADENINE MOLECULE SHOWN)

4x4x4 {100} cleavage bcc Cr electrodes were defined and built for each molecular nucleobase junction as shown in Figure 9, and preliminary calculations are being performed. Does SAIT use CrO2 instead? We will characterize the effect of a larger exposed surface area per electrode, to the translocating ssDNA, compared to the single atom layer GNR electrodes.

MOLECULAR DYNAMICS TRANSLOCATION ACROSS SILICON-GRAPHENE NANOPOROUS MEMBRANE

We performed ssDNA translocation calculations on two different configurations, initially a setup similar to that shown in Figure 1 and subsequently on a newly proposed configuration, which involves am Si3N4 slab sandwiching the GNR electrodes with a gap of 3nm. In the former, we observed once again that the ssDNA interacts strongly through nonbonded forces with the graphene surface in the GNRs. For this reason, we opted for a design that hides the graphene surface from the ssDNA (shown in Figure 10).

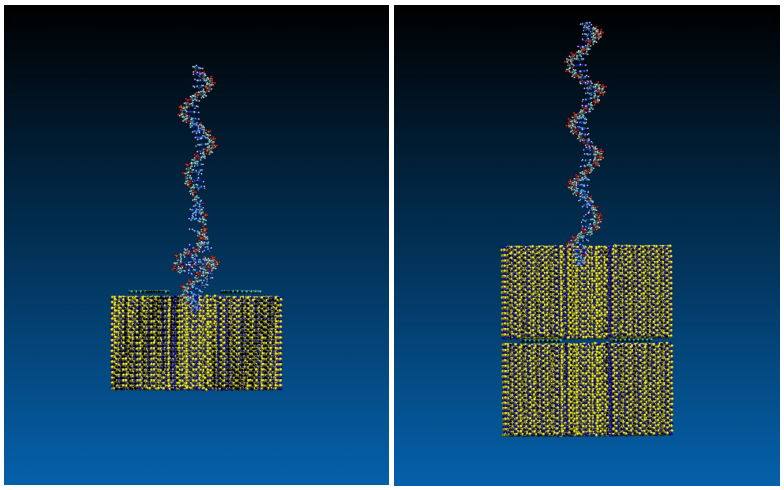

FIGURE 10 (LEFT) ORIGINAL SAIT NANOPORE WITH GNR ELECTRODES DESIGN, AND (RIGHT) GNR-SI3N4 SLAB SANDWICH DEPICTING THE PORED MEMBRANE AND THE SSDNA.

We constructed a crystalline Si3N4 membrane (~10 nm in thickness) from a unit cell of β-Si3N4 crystal. The membrane has a length along the z-axis of 36 Si3N4 unit cells (10.45 nm) and a hexagonal cross section in the xy place of 12 Si3N4 unit cells. A cylindrical pore of 3nm in diameter was produced on the Si3N4 substrate slab. The middle layers of the membrane (z=0) that belong to one unit cell were removed. Two graphene nanoribbon electrode segments were placed at z =0 and separated by 3nm, which is equal to the chosen pore diameter. A 40 basepairs dsDNA helix was built from individual basepairs in the geometry suggested by the Quanta software (Polygen. 1988. Quanta Polygen Corporation, Waltham, MA.). The helix was oriented normal to the membrane and placed 1 nm within the pore. The ssDNA was obtained by removing one of the strands in the dsDNA helix. The system structure is shown in XX. The Si3N4/DNA complex was then solvated in a volume of pre-equilibrated TIP3P water molecules. K+ and Cl- ions were added in proportion to the desired molar concentration, which ranged from 0.01 M to 3 M.

MD simulations were carried out using the program NAMD2 ([10]), with the CHARMM[11] force field describing the Si3N4 nucleic acid, water, graphene and ions, and a custom force-field describing the Si3N4

membrane. The van der Waals parameters and charges of Si3N4 atoms were taken from our group's force field[12]; every Si3N4 atom was restrained by a harmonic force to its initial location in the crystalline membrane with the force constant of 0.01 or 0.1 kcal/(nm2 mol) for bulk and surface atoms, respectively. Graphene layers were also restrained to the Si3N4 surface by a harmonic force using a force constant of 0.05 kcal/(nm2 mol). The spring constant of the harmonic bonds connecting silicon and nitrogen atoms in Si3N4 was adjusted to yield the relative permittivity of bulk Si3N4 of 7.5[13]. The DNA-specific force generating from grid-steered molecular dynamics method[14] is used to reduce the interaction between the DNA and the pore surface and thus prevent irreversible binding of DNA to the pore walls.

We performed 2,000 steps of minimization, or until convergence to 1e-4 in energy difference, followed by a 500 ps NPT simulation to equilibrate the system. We then apply a uniform electric field with 6.5 V along z directions and ran the simulations with the ssDNA translocating through the membrane. In all simulations, the temperature was kept at 295 K by applying Langevin thermostat with the damping constant of 1.0 ps-1.

TRANSLOCATION DYNAMICS AT DIFFERENT IONIC SOLUTION CONCENTRATIONS

From Figure 11 we observe that: 1) there is a sharp change in translocation speed for small increases in concentration, up to 0.1M, 2) there is a concentration sweet-spot that maximizes the translocation speed (between 0.1 and 1.0M), 3) the ssDNA translocates even at low ionic concentrations due to its polar nature, 4) there is a sharp decrease in translocation velocity after the sweet-spot, and the relationship between concentration and speed becomes inversely proportional, and 5) there is non-linearity during initial ssDNA entry into the pore. We believe there is a viscous effect that influences these results, which can be used to control the nucleotide reading sequence rate, and we will explore it further. We also believe the ssDNA-graphene surface nonbond interactions can be reduced significantly at higher concentrations. We will also explore this with the SAIT design.

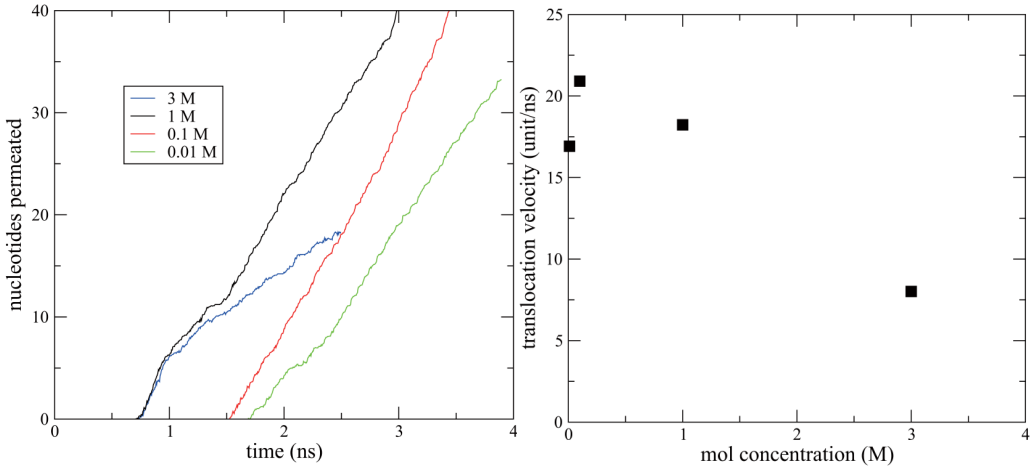

FIGURE 11 (LEFT) NUMBER OF NUCLEOTIDES PASSING THE PORE CENTER AS A FUNCTION OF TIME FOR DIFFERENT IONIC SOLUTION CONCENTRATIONS (3M HAS NOT COMPLETED), AND (RIGHT) ESTIMATED TRANSLOCATION VELOCITY AS A FUNCTION OF MOLAR CONCENTRATION FOR THE IONIC SOLUTION.

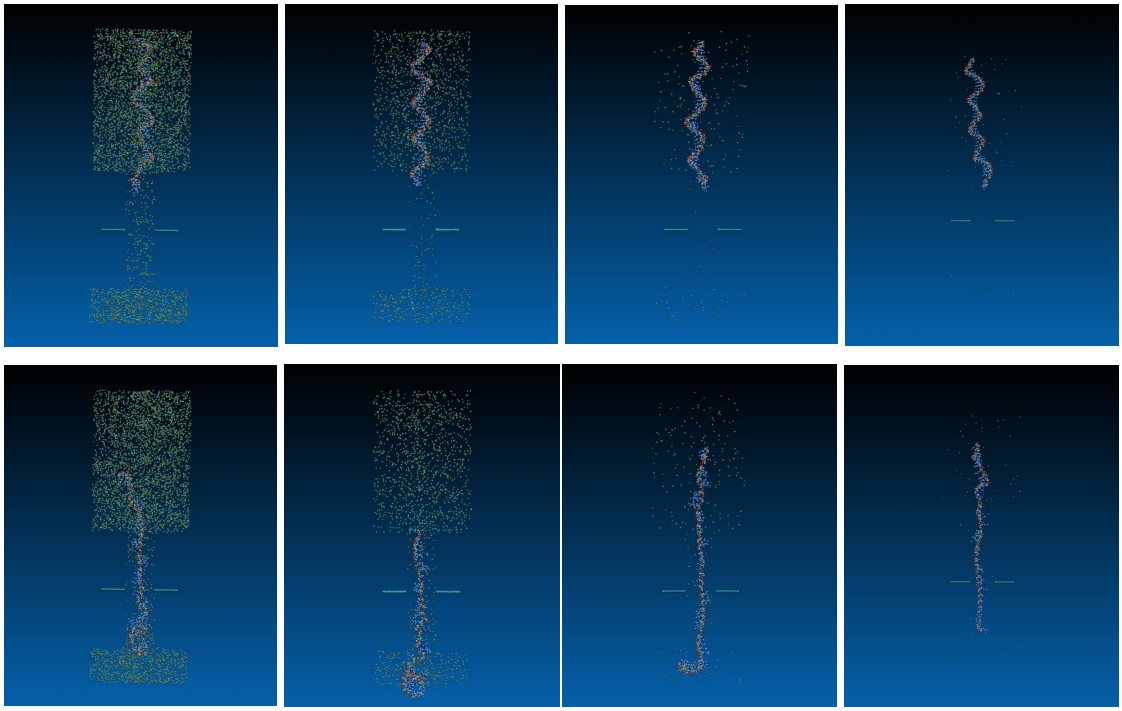

FIGURE 12 SNAPSHOT SEQUENCE OF SSDNA TRANSLOCATION BETWEEN 0 AND 2.5NS VARYING CONCENTRATION, FROM 3M (LEFTMOST) TO 0.01M (RIGHTMOST). SI3N4 SLABS ARE NOT SHOWN; GNR ELECTRODES ARE SHOWN IN THE MIDDLE OF THE SI3N4 SANDWICH.

We will prepare further conclusions as simulations progress.

REFERENCES

1. Jia, X.T., M. Hofmann, V. Meunier, B.G. Sumpter, J. Campos-Delgado, J.M. Romo-Herrera, H.B. Son, Y.P. Hsieh, A. Reina, J. Kong, M. Terrones, and M.S. Dresselhaus, *Controlled Formation of Sharp Zigzag and Armchair Edges in Graphitic Nanoribbons.* Science, 2009. **323**(5922): p. 1701-1705.
2. Nakada, K., M. Fujita, G. Dresselhaus, and M.S. Dresselhaus, *Edge state in graphene ribbons: Nanometer size effect and edge shape dependence.* Physical Review B, 1996. **54**(24): p. 17954-17961.
3. Brey, L. and H.A. Fertig, *Edge states and the quantized Hall effect in graphene.* Physical Review B, 2006. **73**(19).
4. Brey, L. and H.A. Fertig, *Electronic states of graphene nanoribbons studied with the Dirac equation.* Physical Review B, 2006. **73**(23).
5. Kobayashi, Y., K. Fukui, T. Enoki, and K. Kusakabe, *Edge state on hydrogen-terminated graphite edges investigated by scanning tunneling microscopy.* Physical Review B, 2006. **73**(12).
6. Son, Y.W., M.L. Cohen, and S.G. Louie, *Energy gaps in graphene nanoribbons.* Physical Review Letters, 2006. **97**(21).
7. Okada, S., *Energetics of nanoscale graphene ribbons: Edge geometries and electronic structures.* Physical Review B, 2008. **77**(4).
8. Son, Y.W., M.L. Cohen, and S.G. Louie, *Half-metallic graphene nanoribbons.* Nature, 2006. **444**(7117): p. 347-349.
9. Yang, L., C.H. Park, Y.W. Son, M.L. Cohen, and S.G. Louie, *Quasiparticle energies and band gaps in graphene nanoribbons.* Physical Review Letters, 2007. **99**(18).
10. Kale, L., R. Skeel, M. Bhandarkar, R. Brunner, A. Gursoy, N. Krawetz, J. Phillips, A. Shinozaki, K. Varadarajan, and K. Schulten, *NAMD2: Greater scalability for parallel molecular dynamics.* Journal of Computational Physics, 1999. **151**(1): p. 283-312.

11. Brooks, B.R., R.E. Bruccoleri, B.D. Olafson, D.J. States, S. Swaminathan, and M. Karplus, *Charmm - a Program for Macromolecular Energy, Minimization, and Dynamics Calculations.* Journal of Computational Chemistry, 1983. **4**(2): p. 187-217.
12. Wendel, J.A. and W.A. Goddard, *The Hessian Biased Force-Field for Silicon-Nitride Ceramics - Predictions of Thermodynamic and Mechanical-Properties for Alpha-Si3n4.* Journal of Chemical Physics, 1992. **97**(7): p. 5048-5062.
13. Xu, D., J.C. Phillips, and K. Schulten, *Protein response to external electric fields: Relaxation, hysteresis, and echo.* Journal of Physical Chemistry, 1996. **100**(29): p. 12108-12121.
14. Wells, D.B., V. Abramkina, and A. Aksimentiev, *Exploring transmembrane transport through alpha-hemolysin with grid-steered molecular dynamics.* Journal of Chemical Physics, 2007. **127**(12).